Clinical Cancer Research

Preclinical Therapeutic Synergy of MEK1/2 and CDK4/6 Inhibition in Neuroblastoma

Lori S. Hart[1], JulieAnn Rader[1], Pichai Raman[1], Vandana Batra[1], Mike R. Russell[1], Matthew Tsang[1], Maria Gagliardi[1], Lucy Chen[1], Daniel Martinez[2], Yimei Li[1,3], Andrew Wood[1], Sunkyu Kim[4], Sudha Parasuraman[4], Scott Delach[4], Kristina A. Cole[1,3], Shiva Krupa[5], Markus Boehm[5], Malte Peters[5], Giordano Caponigro[4], and John M. Maris[1,3,6]

Abstract

Purpose: Neuroblastoma is treated with aggressive multimodal therapy, yet more than 50% of patients experience relapse. We recently showed that relapsed neuroblastomas frequently harbor mutations leading to hyperactivated ERK signaling and sensitivity to MEK inhibition therapy. Here we sought to define a synergistic therapeutic partner to potentiate MEK inhibition.

Experimental Design: We first surveyed 22 genetically annotated human neuroblastoma-derived cell lines (from 20 unique patients) for sensitivity to the MEK inhibitor binimetinib. After noting an inverse correlation with sensitivity to ribociclib (CDK4/6 inhibitor), we studied the combinatorial effect of these two agents using proliferation assays, cell-cycle analysis, Ki67 immunostaining, time-lapse microscopy, and xenograft studies.

Results: Sensitivity to binimetinib and ribociclib was inversely related ($r = -0.58$, $P = 0.009$). *MYCN* amplification status and expression were associated with ribociclib sensitivity and binimetinib resistance, whereas increased MAPK signaling was the main determinant of binimetinib sensitivity and ribociclib resistance. Treatment with both compounds resulted in synergistic or additive cellular growth inhibition in all lines tested and significant inhibition of tumor growth in three of four xenograft models of neuroblastoma. The augmented growth inhibition was attributed to diminished cell-cycle progression that was reversible upon removal of drugs.

Conclusions: Here we demonstrate that combined binimetinib and ribociclib treatment shows therapeutic synergy across a broad panel of high-risk neuroblastoma preclinical models. These data support testing this combination therapy in relapsed high-risk neuroblastoma patients, with focus on cases with hyperactivated RAS–MAPK signaling. *Clin Cancer Res; 23(7); 1785–96. ©2016 AACR.*

Introduction

Neuroblastoma arises from cells of neural crest lineage in the developing sympathetic nervous system and accounts for 10% of all childhood cancer–related deaths (1). With the development of a comprehensive and aggressive treatment approach, including surgery, chemoradiotherapy, stem cell transplantation, and immunotherapy, cure rates have improved incrementally over time (2). However, relapse occurs in 50% to 60% of high-risk patients, and there is no known curative salvage therapy. This reality underscores the need for novel treatment strategies that include safe and effective therapies to improve cure rates and diminish the long-term side effects caused by cytotoxic chemotherapeutic agents.

We, and others, have shown that multiple genes within the Cyclin D/CDK4/RB axis are altered in primary and relapsed neuroblastomas, including genomic amplification of *CCND1* and *CDK4* and homozygous deletion of the negative regulator *CDKN2A* (3–8). The CDK4 and CDK6 kinases cooperate with Cyclin D family members to activate the E2F transcription factor through the phosphorylation of RB. E2F transcriptional activity results in the stimulation of cell proliferation by promoting progression through the G_1–S cell-cycle checkpoint. Using an RNAi screening strategy targeting the kinome, we independently identified a requirement for CDK4 in the survival and proliferation of neuroblastoma cells (9). Subsequently, we demonstrated efficacy of CDK4 inhibition in neuroblastoma (10) using the small molecule CDK4/6 inhibitor ribociclib (Novartis Oncology), currently in numerous clinical trials both alone and in combination with other novel targeted agents for the treatment of solid tumors.

The MAPK signaling cascade is one of the primary oncogenic pathways attributed to cancer initiation, maintenance, and resistance to therapy. MAPK activation often occurs through mutations and amplifications in upstream receptor tyrosine kinases (*ALK*, *EGFR*, *ERBB2*), mutations in signal transduction genes (*NRAS*, *KRAS*), and/or pathway regulatory genes (*NF1*, *PTPN11*). Although lesions in the canonical MAPK signaling pathway occur in only 3% to 5% of newly diagnosed neuroblastoma specimens

[1]Division of Oncology and Center for Childhood Cancer Research, Children's Hospital of Philadelphia, Philadelphia, Pennsylvania. [2]Division of Pathology, Children's Hospital of Philadelphia, Philadelphia, Pennsylvania. [3]Department of Pediatrics, Perelman School of Medicine at the University of Pennsylvania, Philadelphia, Pennsylvania. [4]Novartis Institutes for Biomedical Research, Cambridge, Massachusetts. [5]Novartis Pharmaceuticals, Basel, Switzerland. [6]Abramson Family Cancer Research Institute, Perelman School of Medicine at the University of Pennsylvania, Philadelphia, Pennsylvania.

Note: Supplementary data for this article are available at Clinical Cancer Research Online (http://clincancerres.aacrjournals.org/).

L.S. Hart and J.A. Rader share first authorship.

Corresponding Author: John M. Maris, Children's Hospital of Philadelphia, 3501 Civic Center Blvd., CTRB 3030, Philadelphia, PA 19104. Phone: 215-590-5244; Fax: 267-426-0685; E-mail: maris@email.chop.edu

doi: 10.1158/1078-0432.CCR-16-1131

Translational Relevance

The mortality associated with neuroblastoma remains significant despite treatment with aggressive multimodal regimens. We have recently shown that MAPK-activating gene alterations are frequent in relapsed disease. Here we evaluated the efficacy of MEK1/2 inhibition (binimetinib; Array BioPharma) across a panel of human neuroblastoma cell lines. Next-generation sequencing of a cancer-specific gene panel and microarray gene expression analysis contributed to the analysis of biomarkers and signatures predictive of response. Sensitivity of neuroblastoma to binimetinib was associated with MAPK-related genomic aberrations and low *MYCN* expression. There was a striking inverse relationship between neuroblastoma cell lines sensitive to binimetinib and those sensitive to CDK4/6 inhibition with ribociclib (Novartis Oncology). Combination of binimetinib and ribociclib showed synergistic G_1 arrest *in vitro*, and improved activity in neuroblastoma xenograft models. These findings support a recently developed clinical trial (NCT02780128) designed to test this combination in relapsed patients with neuroblastoma harboring hyperactivating MAPK mutations.

(11), it is now becoming clear that neuroblastoma genomes evolve extensively under the selective pressure of intensely cytotoxic therapy. For example, *ALK* mutations are significantly enriched in relapse specimens (12). In addition, we recently showed that 78% (18/23) of relapsed neuroblastomas harbor mutations predicted to hyperactivate RAS signaling, and many of these were clonally enriched after the selective pressure of chemoradiotherapy (13).

Because of the expansion of somatic mutations in the relapsed setting and the numerous therapeutic interventions already employed by the time of relapse, the identification of novel drug combinations is of utmost importance. Our primary objective was to identify biomarkers of sensitivity and/or resistance to binimetinib and ribociclib treatment in order to design combination strategies. Here we show that binimetinib and ribociclib activity are inversely related, and that combined binimetinib and ribociclib treatment is synergistic in neuroblastoma cell lines and xenografts with MAPK-hyperactivating mutations or *MYCN* amplification.

Materials and Methods

Cell culture and chemicals

Human-derived neuroblastoma cell lines and the hTERT immortalized, nontransformed RPE-1 cell line were obtained from the Children's Hospital of Philadelphia cell line bank, the Children's Oncology Group, or ATCC and were cultured in RPMI1640 medium containing 10% FBS, 2 mmol/L L-glutamine, and 1% streptomycin/penicillin at 37°C under 5% CO_2. It is important to note that the SY5Y cell line is a subclone of the SK-N-SH line, and the SK-N-BE(2), and SK-N-BE(2)C cell lines were obtained from the same patient before and after chemotherapy, respectively. The genomic identity of each line was confirmed (2015) using the AmpFISTR Identifier Kit (Applied Biosystems), and lines were routinely tested to confirm the lack of mycoplasma contamination. Binimetinib and ribociclib were provided by Novartis and dissolved in DMSO.

Gene expression profiling

Neuroblastoma cell lines were plated in 100-mm dishes and cultured for approximately 48 hours. Messenger RNA was extracted from log-phase cultures using the AllPrep DNA/RNA/Protein Mini Kit (Qiagen). Baseline gene expression profiling was performed (HuGene1.0ST microarrays, Affymetrix, GEO accession GSE78061). See "Statistical analysis" for details on analyses performed.

Foundation medicine profiling

Neuroblastoma cell lines were plated in 100-mm dishes and cultured for 48 hours to roughly 80% confluency. DNA was extracted using the DNEasy Kit (Qiagen). Exome sequencing was performed (Foundation Medicine) on DNA samples according to the Foundation Medicine T5 assay cancer-specific panel.

Cell growth and viability assays

Single-agent activity of binimetinib and ribociclib was determined on a panel of 22 neuroblastoma cell lines and the RPE normal control cell line using the RT-CES (real-time cell electronic sensing) cellular impedance assay (Roche). Briefly, cells were seeded in 96-well plates at roughly 8,000 to 10,000 cells per well depending on growth kinetics and were dosed in triplicate 24 hours later with a four-log dose range (0–10,000 nmol/L) of ribociclib or binimetinib. IC_{50} values were calculated using AUC at time points when cell indexes plateaued indicating confluency (roughly 96 hours posttreatment) as previously described (10).

To assess the combination efficacy of ribociclib and binimetinib, neuroblastoma cell lines ($N = 20$) were seeded in 96-well plates and treated with the combination of binimetinib and ribociclib. Doses used in combination assays were based upon single-agent IC_{50} values determined by CellTiter-Glo: cells were plated at 1,000 to 4,000 cells per well of a 96-well plate and dosed in triplicate 24 hours later with the same dose range of either compound. Viability was measured after 6 days with CellTiter-Glo, and IC_{50} values were calculated as previously described (14). For combination studies, the dose selection included a range from 1/4× to 4× (with × indicating single-agent IC_{50}) and cells were plated in duplicate wells in a matrix format for treatment with both compounds. A select panel of cell lines ($n = 4$) was also treated with binimetinib and ribociclib at low doses of 0, 187, 375, 750, 1,500, and 3,000 nmol/L irrespective of IC_{50}. After 6 days of treatment, cell viability was measured using CellTiter-Glo. Drug synergy was analyzed by isobologram and combination index methods (15), and synergy scores were determined by Chalice (16).

Immunoblots

Whole-cell protein was extracted with lysis buffer containing 150 mmol/L NaCl, 25 mmol/L Tris, 1 mmol/L EDTA, 1 mmol/L EGTA, 1 mmol/L DTT, and 1% Triton X-100 with 1% Halt protease/phosphatase inhibitor (Thermo Scientific, #78440). Protein concentration was determined using the BCA protein assay (Thermo Scientific). Approximately 20 to 40 μg of protein were resolved by SDS-PAGE and were blotted as previously described (10) with the following primary antibodies (Cell Signaling Technology, unless otherwise noted): p-ERK (1:4,000, #4370), ERK (1:4,000, #4695), p-MEK (1:1,000, #9121), MEK (1:1,000, #8727), Ku80 (1:2,000, #2753), PARP (1:1,000, #9542), c-PARP (1:1,000, #5625), RB (1:2,000, #9309), p-RB $S^{807/811}$ (1:1,000, #9308), p-RB^{S795} (1:1,000, #9301), p-RB^{S780}

(1:1,000, #9307), MYCN (1:1,000, #9405), p21 (1:1,000; BD Pharmingen #556430), β-actin (1:5,000; Santa Cruz Biotechnology; #sc-47778). All immunoblots were stained with Ponceau S prior to immunoblotting to confirm equal protein loading between lanes.

Flow cytometry

Cell-cycle analysis. Following treatment at the indicated time points, cells were trypsinized, washed with PBS supplemented with 1% FBS, and fixed overnight at −20 °C with 70% ethanol. Cells were then washed twice, stained with Fx-Cycle Violet (Invitrogen #F10347) according to the manufacturer's protocol, and analyzed on an Attune flow cytometer (Life Technologies). Analysis was performed using FlowJo v10, where cells were gated to exclude non-cell debris and doublets. Proportions of cells in sub-G_1, G_1, S, and G_2–M phases of the cell cycle were then determined using FlowJo's Cell Cycle Univariate Analysis feature and normalized to 100% prior to graphing.

Ki67 staining. After 3 days of treatment with binimetinib, ribociclib, or both, cells were trpysinized, washed with PBS supplemented with 1% FBS, and fixed overnight at −20 °C with 70% ethanol. Cells were washed twice with PBS containing 1% FBS and 0.09% sodium azide (Sigma Aldrich), resuspended in PBS at a concentration of 1×10^6 cells/mL, and stained for 30 minutes at room temperature with 20 μL/mL PE-conjugated Ki67 (BD Biosciences, #51-36525X) or with 20 μL/mL isotype control (BD Biosciences, #51-35405X). The mean fluorescent intensity of stained cells was then measured on an Attune flow cytometer (Life Technologies).

Cell doubling time. Cells suspended in PBS at 1×10^7 cells/mL were stained with 1 mmol/L carboxyfluorescein diacetate succinimidyl ester (CFSE; Invitrogen # C34554) for 10 minutes in the dark at room temperature. Excess dye was quenched by washing cells in culture medium containing 10% FBS. Stained cells were then seeded into 6-well plates and treated 24 hours later with ribociclib, binimetinib, or the combination of ribociclib and binimetinib. Cells were harvested at the time of treatment (0 hours) and daily between 24 and 144 hours after treatment prior to analysis on an Attune flow cytometer (Life Technologies). The loss of CFSE fluorescence was used as a measure of cellular division as CFSE fluorescence is reduced by half within each actively dividing cell (17).

Xenograft studies

Female CB17 SCID$^{-/-}$ mice ages 5 to 7 weeks were obtained from Taconic Biosciences. To evaluate the synergy of binimetinib and ribociclib *in vivo*, neuroblastoma cell line-derived xenografts were implanted subcutaneously into the right flank of each mouse. Animals bearing engrafted tumors of 0.2 to 0.5 cm^3 were then randomized ($n \geq 9$ mice/group) into the following groups for oral treatment: (i) 3 mg/kg binimetinib in 0.1% carboxymethylcellulose/0.5% Tween-80, twice daily; (ii) 75 mg/kg ribociclib in 0.5% methylcellulose, once daily; (iii) 3 mg/kg binimetinib and 75 mg/kg ribociclib; or (iv) vehicle control. Tumor volume was measured throughout treatment using calipers, and was calculated as: volume = $(\pi/6)$(diameter^3), as previously described (18–20). Mice were euthanized when tumor volume reached 3 cm^3, in accordance with CHOP IACUC guidelines (Approved IACUC Protocol #643). A linear mixed-effects model was used to measure differences in tumor growth rates between the vehicle, single agent, and combination groups as described "Statistical analysis."

Immunohistochemistry

Tumors excised from mice after 7 days of treatment were fixed with 10% buffered formalin phosphate (Thermo Fisher Scientific), paraffin embedded, and sectioned for staining of the Ki67 proliferation marker (Abcam #16667). Staining and subsequent imaging were performed as previously described (10).

Statistical analysis

Microarray analysis. All microarray data were processed using robust multiarray procedure (RMA), and quality control metrics were obtained using the "arrayqualitymetrics" package in R. The data were then log2 transformed, and Pearson correlation was performed against IC_{50} values (log10) to find genes significantly associated with sensitivity or resistance to each compound. From the correlation statistic and the sample size, the two-tailed *P* value was calculated for each gene. The *P* values were than adjusted for multiple hypotheses testing using the Benjamini–Hochberg correction. At this point, genes were called significant if their adjusted *P* value was less than 0.25, a cutoff used by Broad GSEA (http://www.broadinstitute.org/cancer/software/gsea/wiki/index.php/FAQ). Gene set *P* values were calculated using the hypergeomtric test, comparing each gene set to the list of genes associated sensitivity. Details about the gene sets including number of genes, source, a description, and actual gene names are captured in the Broad Molecular Signatures Database at the following:

(i) http://software.broadinstitute.org/gsea/msigdb/cards/BIOCARTA_MAPK_PATHWAY (87 genes),
(ii) http://software.broadinstitute.org/gsea/msigdb/cards/BIOCARTA_P38MAPK_PATHWAY (40 genes),
(iii) http://software.broadinstitute.org/gsea/msigdb/cards/RAS_PROTEIN_SIGNAL_TRANSDUCTION (66 genes).

For purposes of differentiating sensitive, intermediate, and refractory to examine correlation between drug response and mutations, the k-means clustering method was used with a setting of three centers ($K = 3$). This method can be used to group sets of observations together in a data-driven manner by partitioning points into *k* groups such that the sum of squares from points to the assigned cluster centers is minimized, thereby eliminating the bias stemming from arbitrary cut-offs. Once observations (IC_{50}s) were assigned to groups the group with the lowest average IC_{50} was called as "sensitive," the group with the highest average IC_{50} was termed the "resistant" group, and the final group was deemed the "intermediate" group. Visualizations including bar charts, heatmaps, Venn diagrams, and scatter plots were created using the "ggplot2," "pheatmap," and "VennDiagram" packages. All data analysis and plots were generated within the R/Bioconductor framework.

Xenograft studies. Linear mixed-effects model was used to test the difference in the rate of tumor volume changing over time between different groups. The model included group, day, and group-by-day interaction as fixed effects, and included a random intercept and a random slope for each mouse. A significant group-by-day interaction suggests that the tumor volume changes at

Table 1. Binimetinib and ribociclib alone and in combination across a human neuroblastoma cell line panel annotated with relevant genomic alterations.

	Binimetinib IC_{50} (nmol/L)	Ribociclib IC_{50} (nmol/L)	Synergy score	NF1	NRAS	KRAS	PTPN11	BRAF	MYCN	ALK	CDK4	CDKN2A	MDM2	TP53
NB-16	5	>10,000	1.20											
NB-EBc1	5	6,400	1.35											
NLF	17	328	2.44											
SK-N-SH	18	148	0.43											
NB-69	24	738	1.05											
CHP-212	26	155	0.781											
SK-N-AS	87	>10,000	0.86											
SK-N-FI	101	3,500	1.01											
SK-N-BE(2)C	159	134	1.28											
NBL-S	170	464	1.30											
NGP	545	175	1.31											
NB-1643	771	147	ND											
SK-N-BE(2)	835	420	1.73											
NB-SD	1,013	1,900	0.68											
SY5Y	1,571	154	ND											
NB-1691	2,092	336	0.74											
LAN5	3,856	429	0.85											
Kelly	7,920	220	1.59											
SMS-SAN	>10,000	250	1.08											
SK-N-DZ	>10,000	801	2.91											
IMR-05	>10,000	126	0.87											
CHP-134	>10,000	273	0.24											

MAPK
MYCN
ALK
CDK4
p53

NOTE: Cell lines are ranked according to binimetinib sensitivity. Genomic analysis was performed according to a focused cancer-associated gene list (Foundation Medicine) with displayed aberrations (copy number loss (*NF-1*), copy number amplification defined as CN > 8 (*BRAF, MYCN, CDK4, MDM2*), and mutations (*NRAS, KRAS, PTPN11, ALK, CDKN2A, TP53*) reduced to genes most commonly altered in neuroblastoma pathogenesis. Synergy values were determined by Chalice analysis of cell survival data obtained from CellTiter-Glo assays using a matrix treatment schedule from 1/4× to 4× IC_{50} (strong synergy >2; synergy >1; additive ~0; ND, not determined).

different rates for the two comparison groups. The model used control group as the reference group and create separate group indicators and interaction terms for other groups. Appropriate contrast statements were created to compare the treatment groups against the control group.

Results and Discussion

Mutation and gene expression analysis of human neuroblastoma cell lines

We utilized next-generation sequencing and gene expression microarrays to identify key driver mutations and biomarkers predictive of response to small-molecule kinase inhibitors targeting CDK4/6 and MEK1/2. To associate the activity of the inhibitors to relevant genomics variables, including gene mutations and copy number alterations, we used a validated cancer-specific gene panel approach (21) in 22 human neuroblastoma cell lines (Table 1 and Supplementary Tables S1 and S2). Finally, for the analysis of differential gene expression patterns predictive of sensitivity to CDK4/6 and MEK1/2 inhibition, we performed gene expression microarray experiments (Affymetrix HuGene1.0ST, GEO accession GSE78061) on RNA isolated from 20 of the cell lines.

Inverse relationship of sensitivity to MEK1/2 and CDK4/6 inhibition

Because of our recent demonstration of an enrichment of MAPK-related genomic lesions in relapsed neuroblastoma (13), we tested the anti-neuroblastoma efficacy of MEK1/2 inhibition with the small-molecule MEK1/2 inhibitor binimetinib. Using real-time cell electronic sensing (RT-CES) technology (10, 22), we analyzed the response of human neuroblastoma cell lines to binimetinib treatment and determined IC_{50} values (Table 1; Supplementary Fig. S1A). We found a wide range of sensitivity to MEK1/2 inhibition *in vitro*, with a median IC_{50} of 545 nmol/L (range 5–>10 μmol/L). Binimetinib treatment resulted in a rapid reduction in the levels of phosphorylated ERK in the majority (but not all) of the sensitive cell lines, and there was minimal modulation apparent in the resistance cells (Supplementary Fig. S1B). As expected, binimetinib treatment induced p21 expression and G_1 accumulation in sensitive neuroblastoma cell lines (Supplementary Fig. S1C and S1D).

In parallel to performing single-agent binimetinib studies, we demonstrated that single-agent CDK4/6 inhibition (ribociclib) shows efficacy in preclinical models of neuroblastoma (10). We were interested in establishing biomarkers predictive of response to binimetinib and ribociclib treatment for the development of criteria for patient selection in future neuroblastoma trials. Strikingly, a direct comparison of the binimetinib and ribociclib IC_{50} values revealed that cell lines most resistant to ribociclib (NB-EBc1, NB-16, SK-N-AS, SK-N-FI) were remarkably susceptible to growth inhibition by binimetinib treatment. Compilation of the aberrations with regards to ranked IC_{50} values provides a visual map of pathway involvement with MAPK alterations associated with binimetinib sensitivity and *MYCN* amplification associated with ribociclib sensitivity (Table 1).

Using the Pearson correlation, we compared gene expression levels against the IC_{50}-generated cell line values for both binimetinib and ribociclib single-agent activity to establish gene lists associated with both sensitivity and resistance to each compound (Supplementary Table S3). We ranked the cell lines according to the IC_{50} values for each compound and the corresponding gene lists cluster into heatmaps demonstrating variable expression according to sensitivity (Fig. 1A and B). The analysis of sensitivity based on gene expression highlights distinct sensitivity profiles for each of the kinase inhibitors suggesting distinct vulnerabilities among the neuroblastoma cell lines.

To further identify whether MAPK pathway mutations and/or *MYCN* amplification was associated with sensitivity to either compound, we used the k-means clustering method to segregate the cell lines into resistant, intermediate, and sensitive groups in an unbiased manner. Binimetinib (but not ribociclib) sensitivity was significantly associated with the presence of MAPK-activating mutations (Fig. 1C). Consistent with our previously analysis of single-agent ribociclib, we found that ribociclib sensitivity (but not binimetinib) significantly associated with the presence of *MYCN* amplification (Fig. 1D; ref. 10). Sensitivity to either compound was independent of *ALK* and *TP53* mutation status (Supplementary Fig. S2A and S2B).

We observed that many of the lines most sensitive to binimetinib were lacking *MYCN* amplification. These models (NB-EBc1, NB-16, SK-N-AS, SK-N-FI) demonstrate extreme resistance to ribociclib, an observation we previously reported (10). To further explore the significance of this relationship, we evaluated the correlation of sensitivity to each compound with regards to *MYCN* amplification status and *MYCN* expression level. Neuroblastoma models characterized by *MYCN* amplification or increased *MYCN* expression were significantly more sensitive to ribociclib and resistant to binimetinib (Fig. 2A–C). This inverse relationship is explained, at least in part, by the inverse correlation of MYCN protein levels with phosphorylated ERK. Although increased MYCN protein levels trended with binimetinib resistance (high IC_{50s}, right side of immunoblots), increased ERK activation was associated with binimetinib sensitivity (low IC_{50s}, left side of immunoblots; Fig. 2D). Low levels of NF1, a negative regulator of MAPK, was also associated with sensitivity to binimetinib, a finding that corroborates similar studies recently reported by Woodfield and colleagues (23). Activation status of MEK itself did not appear correlated with sensitivity to MEK1/2 inhibition, consistent with previous studies (24). Finally, as we have previously demonstrated, levels of CDK4 and activation status of Rb were not associated with sensitivity to ribociclib (10).

In addition, using three different published MAPK gene sets we observed a significant association of each with sensitivity to binimetinib (BIOCARTA_MAPK_PATHWAY $P = 0.007$; BIOCARTA_P38MAPK_PATHWAY $P = 0.001$; RAS_PROTEIN_SIGNAL_-TRANSDUCTION $P = 0.009$). Although sensitivity to each compound correlated directly (ribociclib) and inversely (binimetinib) with *MYCN* amplification status and expression level, gene-set enrichment analysis of the sensitivity gene lists did not identify previously reported *MYC*/*MYCN* signatures (25, 26). Therefore, although associated with *MYCN* expression, sensitivity to MEK1/2 and CDK4/6 inhibitors is not explained by downstream *MYC*/*MYCN* effectors.

Synergistic interaction of MEK1/2 and CDK4/6 inhibitors

To test the synergistic effects of combined binimetinib and ribociclib treatment in neuroblastoma, we performed cell proliferation assays based on the quantification of ATP. The combination treatments were performed in a matrix design across a range of doses for each compound determined by single-agent IC_{50} values previously described (Table 1). More than half of the cell lines tested ($N = 12/20$) demonstrated synergy to the combination with the remaining lines showing additivity. Because of the relative resistance of each cell line to one of the two compounds, we also tested four models at a low dose range of each compound. We chose two models with single copy *MYCN*, deleterious MAPK pathway alterations, and demonstrated sensitivity to binimetinib [NB-EBc1 (mutant *KRAS* and copy number loss of *NF1*) and NBL-S (copy number loss of *NF1*)] and two ribociclib-sensitive models with amplified *MYCN* and *CDK4*-related aberrations [NGP (*CDK4* amplification) and SK-N-BE(2)C (*CDKN2A* mutation)]. The percent affected was calculated from the surviving fraction at each dose combination followed by a Loewe conversion to determine synergy of the combination based on excess inhibition beyond that achieved over the maximum single-agent additive response (16). Consistent with recent findings in *KRAS*-mutant colorectal cancer models, isobologram analysis of the four neuroblastoma models shown in Fig. 3A demonstrate synergy at low doses (Table 1; Fig. 3A; ref. 27). As expected, the combination of binimetinib and ribociclib reduces the activation of both MAPK and RB pathway effectors (Fig. 3B). Although the inhibition of phosphorylated ERK appears similar between single agent and combination treatments, phosphorylated Rb decreased to a greater extent and at lower doses when ribociclib was combined with binimetinib. The augmented inhibition of Rb we observed is consistent with reports of combined MEK1/2 and CDK4/6 inhibition in pancreatic and colorectal cancer models (28, 29). Therefore, MEK1/2 inhibition promotes the effects of ribociclib on cell-cycle inhibition, suggesting MAPK signaling at least partially confers resistance to ribociclib in neuroblastoma.

Under single-agent conditions, both compounds induced a G_1 delay with binimetinib also inducing modest levels of apoptosis in some cell lines (Fig. 4A and Supplementary Figs. S1D, S3A, and S3B; ref. 10). Therefore, we were interested in determining the effects on cell-cycle progression under combined binimetinib and ribociclib treatment. We found near complete accumulation in G_1 induced by the combination at IC_{50} dosing for each compound (Fig. 4A) with similar results observed with as little as $1/4\times$-IC_{50} doses. As an extension of cell-cycle analyses, we measured the doubling rate of cells treated with either single agent or the combination using CFSE cell-labeling assay in conjunction with flow cytometry. The combination of binimetinib and ribociclib decreased the rate of CFSE loss suggesting the proliferation rate of the cells was reduced, and the doubling time subsequently increased (Fig. 4B). We also measured the proliferation marker Ki67 and found a striking reduction in Ki67 in cells treated with both binimetinib and ribociclib compared with the effects observed with either single agent (Fig. 4C). Of note, a small percentage of $Ki67^{HI}$ cells appear to persist, a finding potentially related to the observed reversibility of the cell-cycle arrest (Supplementary Fig. S4). A modest induction of markers of apoptosis (PARP cleavage, sub-G_1 content sensitive to the caspase-inhibitory peptide Q-VD-OPh) was observed, but appeared associated with binimetinib treatment and limited to a subset of cell lines (NBL-S, SK-N-BE(2)C; Supplementary Fig. S3A and S3B).

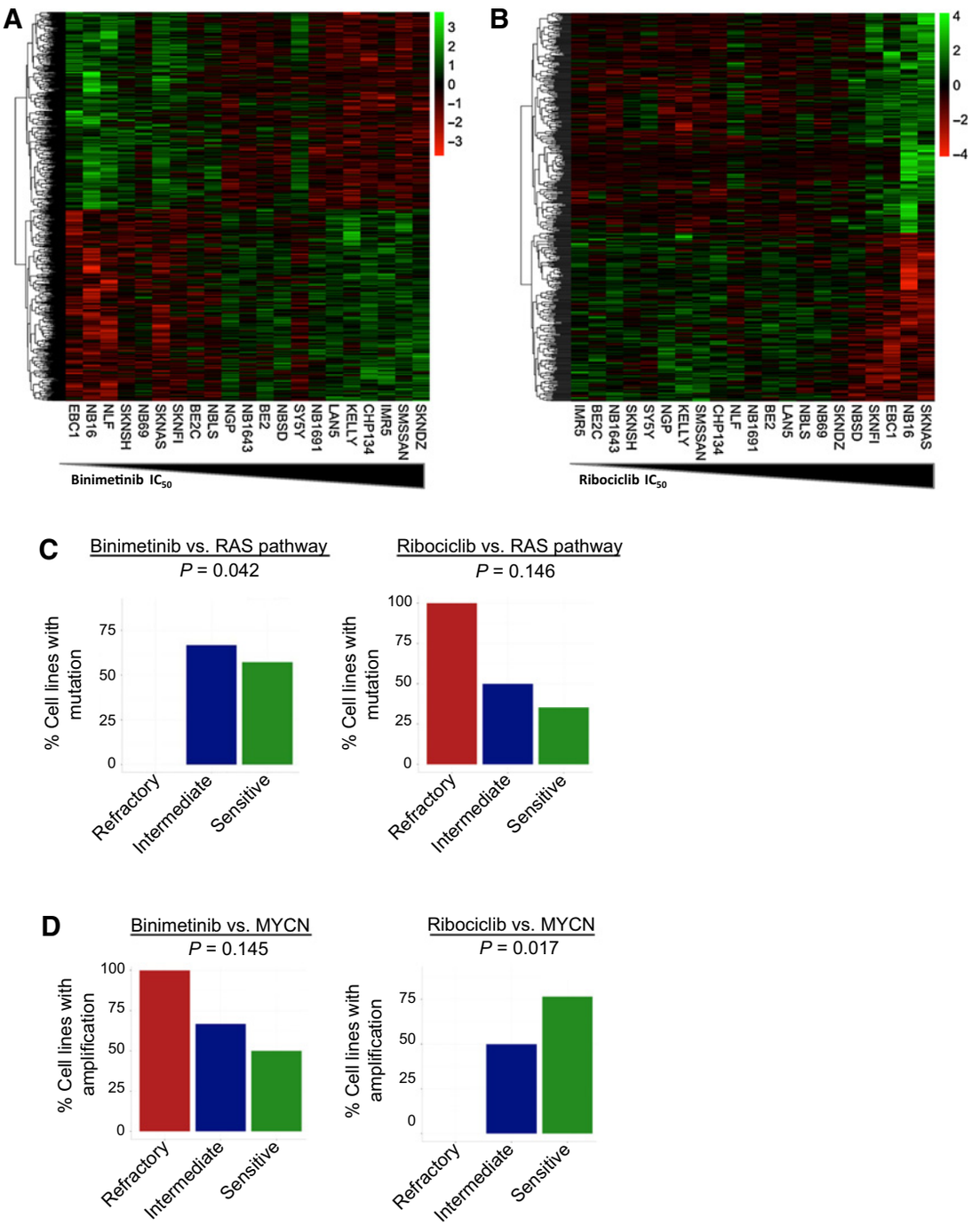

Figure 1.

Gene expression profiling of human neuroblastoma cell lines with regards to relative sensitivity to MEK1/2 and CDK4/6 inhibition. HuGene1.0ST microarrays were performed on a panel of human neuroblastoma cell lines ($N = 21$). **A** and **B,** Heatmap visualizations of differentially expressed genes according to cell line rankings based on IC_{50} values (represented by wedges) of (**A**) binimetinib and (**B**) ribociclib; **C** and **D,** k-means clustering of cell line IC_{50} values to identify associations between the presence of relevant genomic alterations and sensitivity to binimetinib and ribociclib: **C,** RAS–MAPK pathway (binimetinib, $P = 0.042$) and (**D**) *MYCN* amplification (ribociclib, $P = 0.017$).

Although senescence was determined to be a factor in ribociclib single-agent activity (10), we did not observe an increased contribution of senescence following combination binimetinib–ribociclib treatment (Supplementary Fig. S3C), and future experimentation will focus on defining the mechanistic basis of the therapeutic synergy observed here.

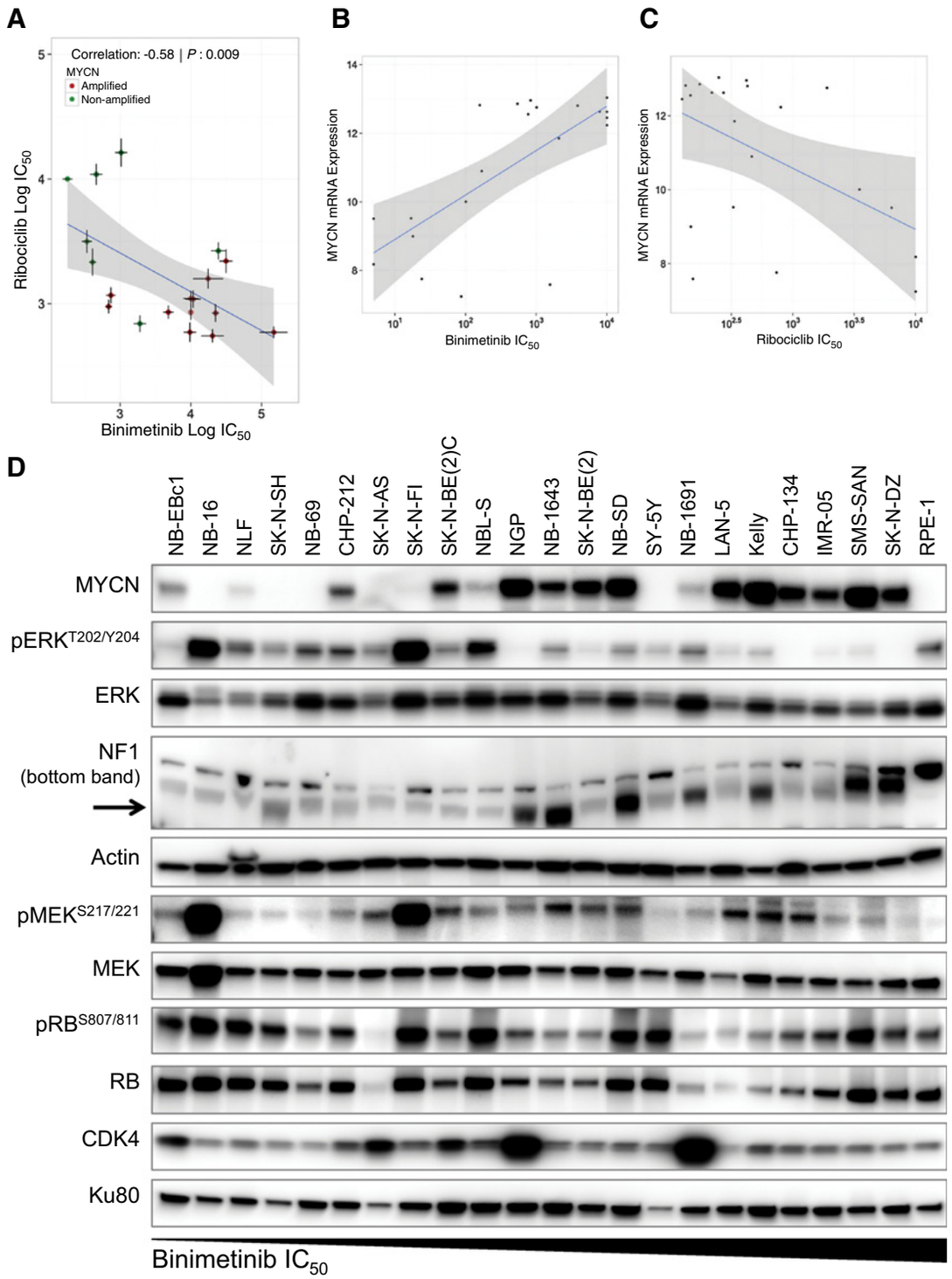

Figure 2.

Inverse relationship of binimetinib and ribociclib sensitivity with regards to *MYCN* amplification and expression. **A,** Inverse relationship of binimetinib and ribociclib (Pearson $r = -0.58$, $P = 0.009$) according to IC_{50} values ($N = 19$) obtained from CellTiter-Glo assays used for combination studies, *MYCN* amplification status annotated (note: CHP-212 excluded from analysis due to high sensitivity and significant apoptosis induced by all compounds tested); **B** and **C,** *MYCN* expression levels plotted against IC_{50} values (nmol/L) for (**B**) binimetinib (Pearson $r = 0.698$, $P = 4.35 \times 10^{-4}$) and (**C**) ribociclib (Pearson $r = -0.496$, $P = 0.022$); and (**D**) immunoblots of MAPK and Cyclin D/CDK4/RB pathway proteins with cell lines ranked according to binimetinib sensitivity (wedge denotes binimetinib IC_{50} ranking); actin and Ku80 are included as loading controls.

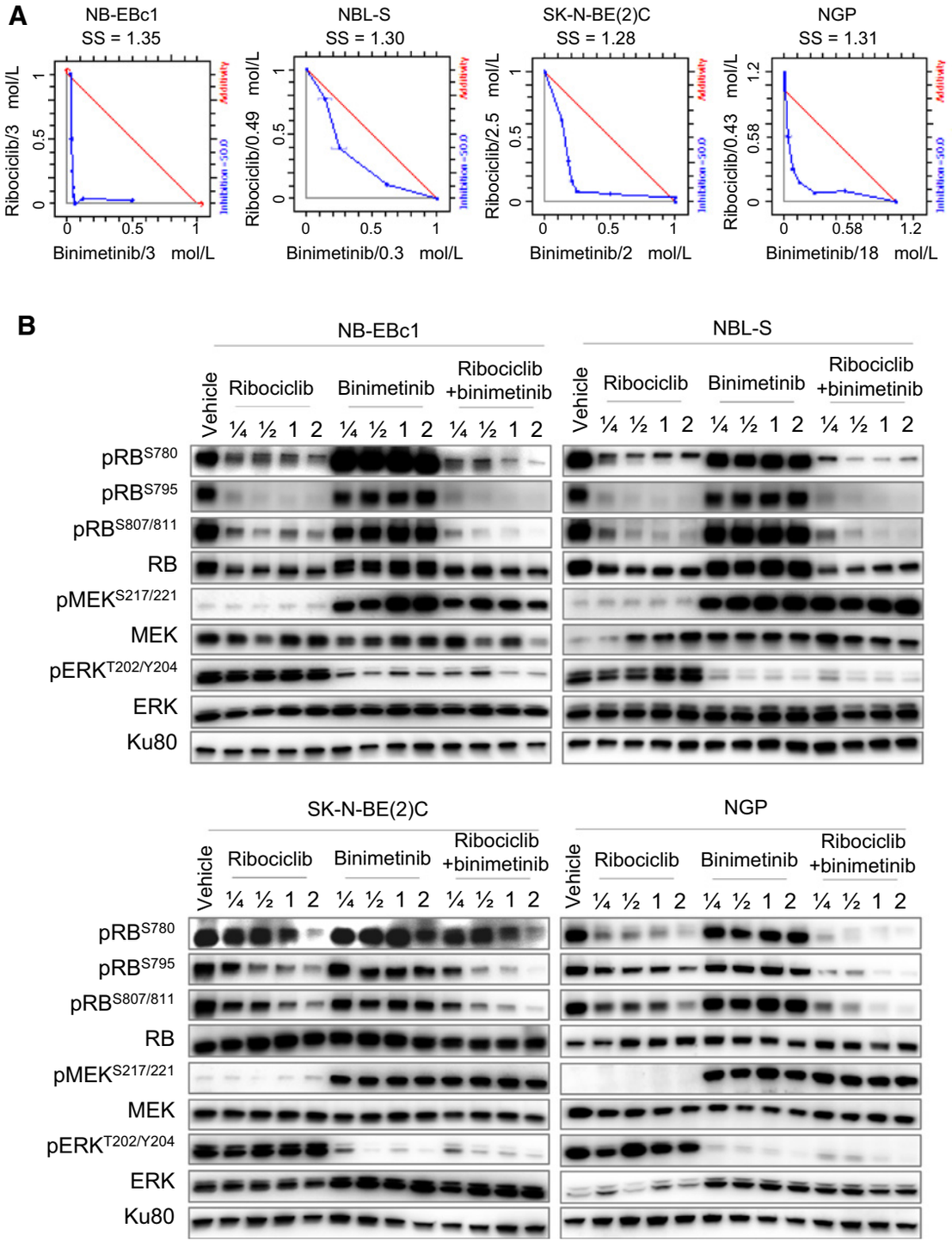

Figure 3.

Neuroblastoma cell lines show a synergistic response to combined MEK1/2 and CDK4/6 inhibition. **A,** Isobologram plots for select neuroblastoma cell lines treated with both binimetinib and ribociclib and (**B**) immunoblot analysis of MAPK and CyclinD/CDK4/RB pathway effectors in response to binimetinib–ribociclib combination treatment; Ku80 is included as loading controls.

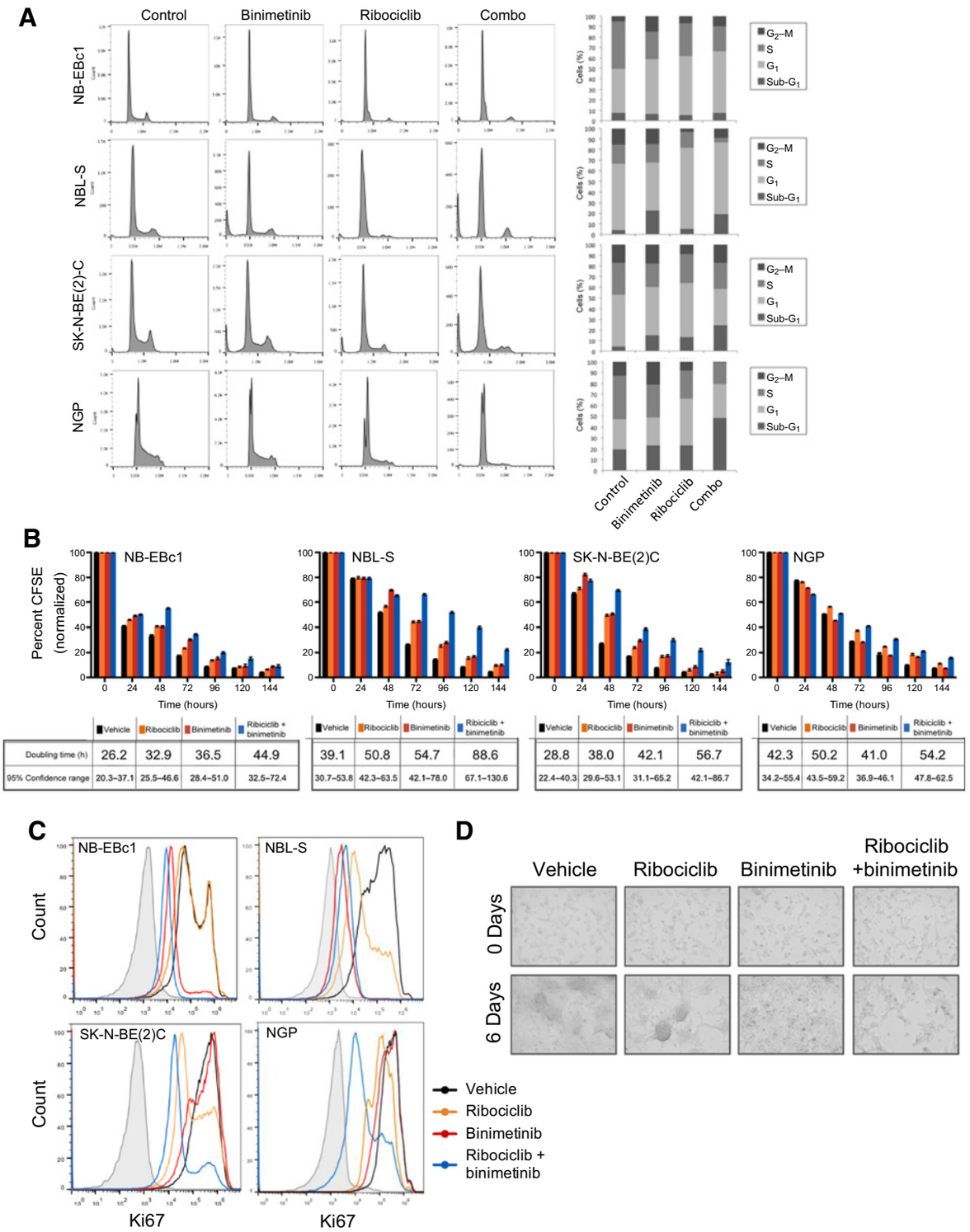

Figure 4.

Combined MEK1/2 and CDK4/6 inhibition induces near complete accumulation in G1. **A,** Cell-cycle analysis of single agent and combined binimetinib and ribociclib treatment (1× IC_{50} doses at 72 hours, quantification on far right from a single dataset representative of three independent experiments); **B,** CFSE analysis and corresponding doubling times (analysis was repeated in at least three independent experiments with representative plots from one experiment shown); **C,** Ki67 staining of treated cells (1× IC_{50} doses at 72 hours); and (**D**) time-lapse microscopy images taken from NBL-S cells treated with binimetinib and ribociclib (1/2× IC_{50}).

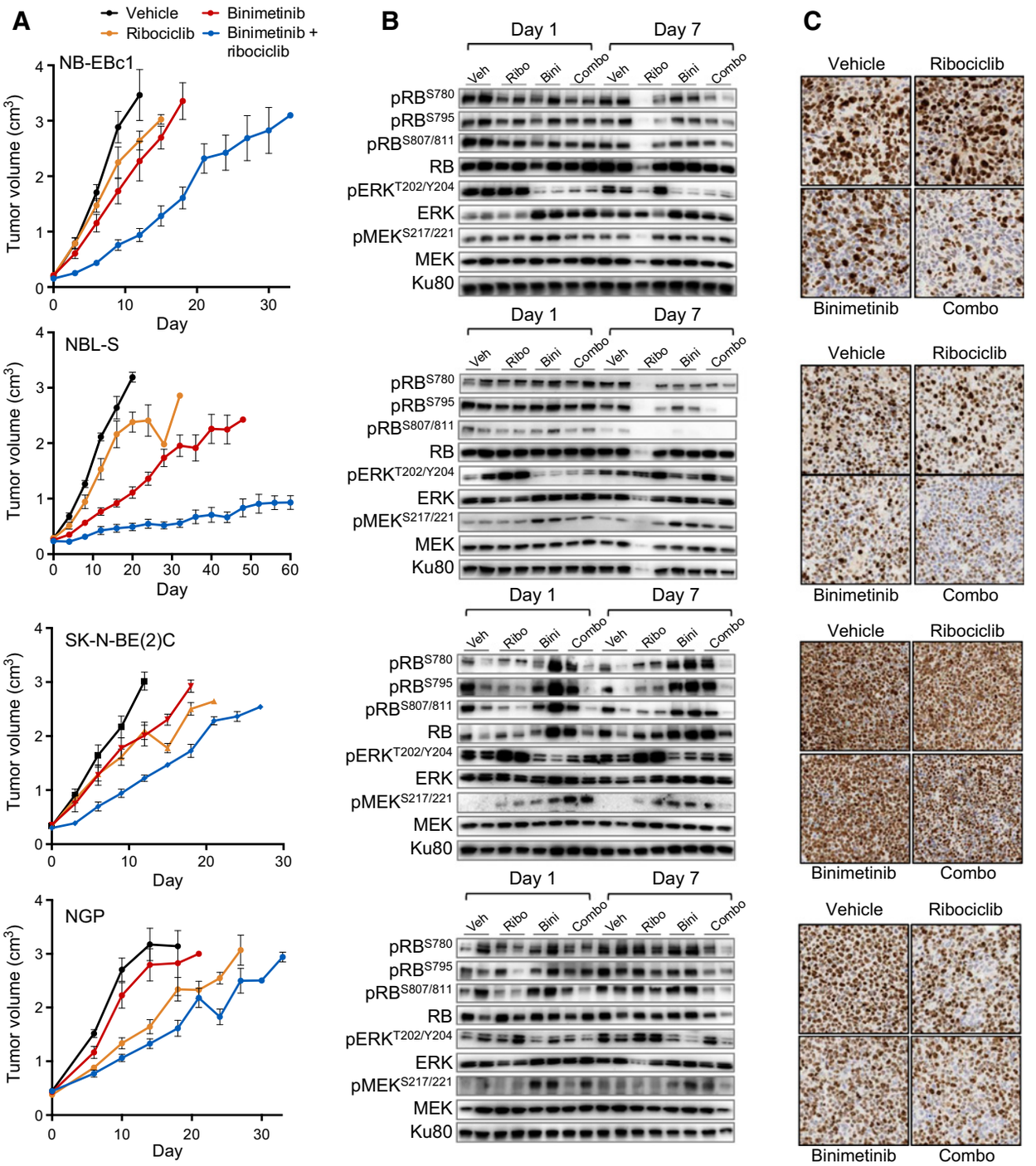

Figure 5.

Neuroblastoma xenografts are sensitive to combined binimetinib and ribociclib treatment. Xenografts were treated with vehicle, single-agent binimetinib (3 mg/kg twice a day), single-agent ribociclib (75 mg/kg every day), or the combination. **A,** Tumor growth delay, **B,** MAPK and RB signaling immunoblots, and **(C)** Ki67 immunohistochemical staining are shown for each model tested. Linear mixed-model statistics were performed as described in the methods. Comparing the combination treatments to the closest single-agent study groups: NB-EBc1 ($P = 0.0003$), NBL-S ($P < 0.0001$), SK-N-BE(2)C ($P = 0.0129$), and NGP ($P = 0.1214$).

To visualize any potential temporal differences of cell growth inhibition between single agent and combination treatments, we performed time-lapse microscopy and imaged identical fields of NBL-S cells treated over the course of 6 days. We observed a difference in cell growth and overall confluency in as little as 48 hours, with a more distinct difference observed at 72 hours and beyond (Fig. 4D). Combined binimetinib and ribociclib treatment induces G_1 accumulation faster and to a larger extent than either single agent alone. However, the cell-cycle arrest was found to be reversible given that the cell lines re-established their baseline cell-cycle profiles within 3 days following removal of the drugs (Supplementary Fig. S4). This finding suggests that ultimately this combination may be most useful in the maintenance stage of treatment when patients with high-risk disease who have achieved a complete response to chemotherapy, but are presumed to harbor chemotherapy-resistant minimal residual disease, are treated with the retinoid isotretinoin in combination with an anti-GD2-directed immunotherapeutic approach to prevent relapse (30).

To identify whether MAPK-activating mutations and/or *MYCN* amplification were associated with synergy, we segregated the cell lines into synergistic and nonsynergistic groups based on synergy score. Synergy was independent of the presence of genomic alterations within the MAPK pathway, *MYCN*, *ALK*, *or TP53* (Table 1; Supplementary Fig. S5). This suggests that patients with *MYCN*-amplified neuroblastoma may benefit from the combination of ribociclib and binimetinib despite the predicted response to either single agent.

Efficacy of combined MEK1/2 and CDK4/6 inhibitors in murine xenotransplantation models

Given the significant synergy demonstrated with combined binimetinib–ribociclib treatment *in vitro*, we sought to test the efficacy of the combination in neuroblastoma xenograft models (18–20). Neuroblastoma xenografts were implanted subcutaneously and allowed to grow to approximately 200 mm^3 at which point they were randomized to one of four treatment arms: vehicle (daily), binimetinib (twice daily, 3 mg/kg), ribociclib (daily, 75 mg/kg), or the combination of binimetinib–ribociclib. Treatments continued daily without holiday until tumor burden endpoints were reached. We observed tumor growth delay by single-agent binimetinib [NB-EBc1 $P = 0.001$, NBL-S $P < 0.0001$, SK-N-BE(2)C $P = 0.0002$, NGP $P = 0.0962$] and ribociclib [NB-EBc1 $P = 0.0256$, NBL-S $P = 0.0065$, SK-N-BE(2)C $P < 0.0001$, NGP $P < 0.0001$] treatments compared with vehicle treatment (Fig. 5A and Supplementary Fig. S6). These results are consistent with the relative *in vitro* sensitivity of the models (Table 1). Combined binimetinib and ribociclib treatment contributed to additional tumor growth delay and prolonged survival beyond single-agent treatment without toxicity (Fig. 5A and Supplementary Fig. S6). All four models showed a significant difference between combination and vehicle treatment groups ($P < 0.0001$), three models showed significant differences between the combination and closest single agent arms [NB-EBc1 $P = 0.0003$, NBL-S $P < 0.0001$, SK-N-BE(2)C $P = 0.0129$], and one of the four models (NBL-S) showed stable disease. The modest effect of combination treatment and progressive disease observed in NB-EBc1, SK-N-BE(2)C, and NGP xenografts may be attributed to the particularly rapid growth rate of these models, as well as the presence of *TP53* mutations [SK-N-BE(2)C and NGP], a characteristic not common in primary human neuroblastomas (31).

All four models showed reduced phosphorylation of ERK and RB after 7 days of therapy according to treatment with binimetinib and ribociclib, respectively (Fig. 5B). Combination treatment resulted in similar inhibition of ERK phosphorylation and additional inhibition of Rb phosphorylation compared to that observed with either single agent and consistent with the effects observed *in vitro*. We observed a reduction in Ki67 staining in tumors treated with the combination, also consistent with our *in vitro* results (Figs. 4C and 5C).

Translational potential of combined binimetinib–ribociclib treatment in neuroblastoma

The treatment of recurrent neuroblastoma is complicated by the inherently aggressive nature of therapy-resistant disease and the limited novel therapy options available at the time of relapse. The presence of newly acquired and/or clonally selected genomic alterations in relapsed disease offers an opportunity for the development of novel treatment (13, 32). The challenge lies in the identification of pathway(s) most important to the survival of the tumors in question. Here we have shown that binimetinib and ribociclib are inversely related with regards to drug sensitivity and *MYCN* amplification status and expression in neuroblastoma cell lines. The combination of the two compounds induces synergistic growth inhibition *in vitro*, often with cells highly resistant to one of the agents becoming sensitive to the combination at exposure levels expected to be achievable in the clinic. In addition, the binimetinib–ribociclib combination showed significant tumor growth delay *in vivo*. Tumor regressions were not achieved in the models tested here, suggesting that more potent inhibitors driving cells toward programmed cell death or irreversible senescence may be required to achieve significant clinical activity in the setting of bulk disease.

This "novel–novel" drug combination challenges the straightforward notion of biomarker-based patient enrichment strategies used for single-agent studies. For example, the correlations of binimetinib response in cells harboring mutations in the RAS–MAPK pathway and ribociclib sensitivity based on *MYCN* amplification and expression status are obscured when ranking synergy scores. However, synergy is a notoriously difficult phenotype to quantify, and patient response data will be required to clarify which genetic lesions robustly predict for response of the combination. Importantly, binimetinib and ribociclib have shown nonoverlapping toxicities in clinical trials to date, suggesting that they could be safely combined in children with neuroblastoma. We suggest that next-generation sequencing results should drive the selection of patients for this combination, particularly for tumors with aberrations predicted to hyperactivate RAS–MAPK signaling. A clinical trial to test this hypothesis, and to explore whether or not the most common somatic alterations in the relapsed neuroblastoma genome can predict response to targeted therapy, has been designed based in part on the data presented herein (NCT02780128).

Disclosure of Potential Conflicts of Interest

M. Peters holds ownership interest (including patents) in Novartis. J.M. Maris reports receiving commercial research grants from Novartis. No potential conflicts of interest were disclosed by the other authors.

Authors' Contributions

Conception and design: L.S. Hart, J.A. Rader, V. Batra, A. Wood, S. Parasuraman, S. Krupa, M. Boehm, M. Peters, G. Caponigro, J.M. Maris

Development of methodology: L.S. Hart, J.A. Rader, V. Batra, M.R. Russell, L. Chen, A. Wood, S. Krupa, J.M. Maris
Acquisition of data (provided animals, acquired and managed patients, provided facilities, etc.): L.S. Hart, J.A. Rader, V. Batra, M.R. Russell, M. Tsang, M. Gagliardi, L. Chen, D. Martinez, K.A. Cole
Analysis and interpretation of data (e.g., statistical analysis, biostatistics, computational analysis): L.S. Hart, J.A. Rader, P. Raman, V. Batra, L. Chen, Y. Li, S. Kim, S. Parasuraman, S. Delach, M. Boehm, M. Peters, G. Caponigro, J.M. Maris
Writing, review, and/or revision of the manuscript: L.S. Hart, J.A. Rader, V. Batra, D. Martinez, Y. Li, S. Parasuraman, M. Boehm, G. Caponigro, J.M. Maris
Administrative, technical, or material support (i.e., reporting or organizing data, constructing databases): L.S. Hart, P. Raman, J.M. Maris
Study supervision: L.S. Hart, M. Peters, G. Caponigro, J.M. Maris

Grant Support

This work was supported by a commercial research grant with Novartis (to J.M. Maris), the Giulio D'Angio Endowed Chair (to J.M. Maris), and foundation research grants from the Cookies for Kids' Cancer Foundation (to J.M. Maris and L.S. Hart), the Arms Wide Open Foundation (to J.M. Maris), the Rally Foundation (to J.M. Maris), and the Alex's Lemonade Stand Foundation (to J.M. Maris).

The costs of publication of this article were defrayed in part by the payment of page charges. This article must therefore be hereby marked *advertisement* in accordance with 18 U.S.C. Section 1734 solely to indicate this fact.

Received May 5, 2016; revised August 29, 2016; accepted September 20, 2016; published OnlineFirst October 11, 2016.

References

1. Smith MA, Seibel NL, Altekruse SF, Ries LA, Melbert DL, O'Leary M, et al. Outcomes for children and adolescents with cancer: challenges for the twenty-first century. J Clin Oncol 2010;28:2625–34.
2. Maris JM. Recent advances in neuroblastoma. N Engl J Med 2010;362: 2202–11.
3. Easton J, Wei T, Lahti JM, Kidd VJ. Disruption of the Cyclin D/cyclin-dependent kinase/INK4/retinoblastoma protein regulatory pathway in human neuroblastoma. Cancer Res 1998;58:2624–32.
4. Krasnoselsky AL, Whiteford CC, Wei JS, Bilke S, Westermann F, Chen Q-R, et al. Altered expression of cell cycle genes distinguishes aggressive neuroblastoma. Oncogene 2004;24:1533–41.
5. Molenaar JJ, Ebus ME, Koster J, Sluis PV, van Noesel CJM, Versteeg R, et al. Cyclin D1 and CDK4 activity contribute to the undifferentiated phenotype in neuroblastoma. Cancer Res 2008;68:2599–09.
6. Molenaar JJ, Koster J, Ebus ME, van Sluis P, Westerhout EM, de Preter K, et al. Copy number defects of G1-cell cycle genes in neuroblastoma are frequent and correlate with high expression of E2F target genes and a poor prognosis. Genes Chromosomes Cancer 2012;51:10–9.
7. Molenaar JJ, van Sluis P, Boon K, Versteeg R, Caron HN. Rearrangements and increased expression of cyclin D1 (CCND1) in neuroblastoma. Genes Chromosomes Cancer 2003;36:242–9.
8. Mosse YP, Diskin SJ, Wasserman N, Rinaldi K, Attiyeh EF, Cole K, et al. Neuroblastomas have distinct genomic DNA profiles that predict clinical phenotype and regional gene expression. Genes Chromosomes Cancer 2007;46:936–49.
9. Cole KA, Huggins J, Laquaglia M, Hulderman CE, Russell MR, Bosse K, et al. RNAi screen of the protein kinome identifies checkpoint kinase 1 (CHK1) as a therapeutic target in neuroblastoma. Proc Natl Acad Sci 2011;108: 3336–41.
10. Rader J, Russell MR, Hart LS, Nakazawa MS, Belcastro LT, Martinez D, et al. Dual CDK4/CDK6 inhibition induces cell-cycle arrest and senescence in neuroblastoma. Clin Cancer Res 2013;19:6173–82.
11. Pugh TJ, Morozova O, Attiyeh EF, Asgharzadeh S, Wei JS, Auclair D, et al. The genetic landscape of high-risk neuroblastoma. Nat Genet 2013;45: 279–84.
12. Schleiermacher G, Javanmardi N, Bernard V, Leroy Q, Cappo J, Rio Frio T, et al. Emergence of new ALK mutations at relapse of neuroblastoma. J Clin Oncol 2014;32:2727–34.
13. Eleveld TF, Oldridge DA, Bernard V, Koster J, Daage LC, Diskin SJ, et al. Relapsed neuroblastomas show frequent RAS-MAPK pathway mutations. Nat Genet 2015;47:864–71.
14. Russell MR, Levin K, Rader J, Belcastro L, Li Y, Martinez D, et al. Combination therapy targeting the Chk1 and wee1 kinases shows therapeutic efficacy in neuroblastoma. Cancer Res 2013;73:776–84.
15. Chou T, Talalay P. Quantitative analysis of dose-effect relationships: the combined effects of multiple drugs or enzyme inhibitors. Adv Enzyme Regul 1984;22:27–55.
16. Lehàr J, Krueger AS, Avery W, Heilbut AM, Johansen LM, Price ER, et al. Synergistic drug combinations improve therapeutic selectivity. Nat Biotechnol 2009;27:659–66.
17. Quah BJC, Parish CR. The use of carboxyfluorescein diacetate succinimidyl ester (CFSE) to monitor lymphocyte proliferation. J Vis Exp 2010:2259.
18. Batra V, Maris JM, Kang MH, Reynolds CP, Houghton PJ, Alexander D, et al. Initial Testing (Stage 1) of SGI-1776, a PIM1 Kinase Inhibitor, by the Pediatric Preclinical Testing Program. Pediatric Blood Cancer 2012;59: 749–52.
19. Keshelava N, Houghton PJ, Morton CL, Lock RB, Carol H, Keir ST, et al. Initial testing (Stage 1) of vorinostat (SAHA) by the pediatric preclinical testing program. Pediat Blood Cancer 2009;53:505–8.
20. Wood AC, Maris JM, Gorlick R, Kolb EA, Keir ST, Reynolds CP, et al. Initial testing (Stage 1) of the antibody-maytansinoid conjugate, IMGN901 (Lorvotuzumab Mertansine), by the pediatric preclinical testing program. Pediat Blood Cancer 2013;60:1860–7.
21. Frampton GM, Fichtenholtz A, Otto GA, Wang K, Downing SR, He J, et al. Development and validation of a clinical cancer genomic profiling test based on massively parallel DNA sequencing. Nat Biotechnol 2013;31: 1023–31.
22. Atienza JM, Zhu J, Wang X, Xu X, Abassi Y. Dynamic monitoring of cell adhesion and spreading on microelectronic sensor arrays. J Biomol Screen 2005;10:795–805.
23. Woodfield SE, Zhang L, Scorsone KA, Liu Y, Zage PE. Binimetinib inhibits MEK and is effective against neuroblastoma tumor cells with low NF1 expression. BMC Cancer 2016;16:1–10.
24. Baranski Z, Booij TH, Kuijjer ML, de Jong Y, Cleton-Jansen A-M, Price LS, et al. MEK inhibition induces apoptosis in osteosarcoma cells with constitutive ERK1/2 phosphorylation. Genes Cancer 2015; 6:503–12.
25. Fredlund E, Ringnér M, Maris JM, Påhlman S. High Myc pathway activity and low stage of neuronal differentiation associate with poor outcome in neuroblastoma. Proc Natl Acad Sci 2008;105:14094–9.
26. Valentijn LJ, Koster J, Haneveld F, Aissa RA, van Sluis P, Broekmans ME, et al. Functional MYCN signature predicts outcome in neuroblastoma irrespective of MYCN amplification. Proc Natl Acad Sci 2012;109: 19190–5.
27. Ziemke EK, Dosch JS, Maust JD, Shettigar A, Sen A, Welling TH, et al. Sensitivity of KRAS-mutant colorectal cancers to combination therapy that cotargets MEK and CDK4/6. Clin Cancer Res 2016;22: 405–14.
28. Franco J, Witkiewicz AK, Knudsen ES. CDK4/6 inhibitors have potent activity in combination with pathway selective therapeutic agents in models of pancreatic cancer. Oncotarget 2014;5:6512–25.
29. Lee MS, Helms TL, Feng N, Gay J, Chang QE, Tian F, et al. Efficacy of the combination of MEK and CDK4/6 inhibitors *in vitro* and *in vivo* in KRAS mutant colorectal cancer models. Oncotarget 2016;7: 39595–608.
30. Yu AL, Gilman AL, Ozkaynak MF, London WB, Kreissman SG, Chen HX, et al. Anti-GD2 antibody with GM-CSF, interleukin-2, and isotretinoin for neuroblastoma. The N Engl J Med 2010;363: 1324–34.
31. Diskin SJ, Capasso M, Diamond M, Oldridge DA, Conkrite K, Bosse KR, et al. Rare variants in TP53 and susceptibility to neuroblastoma. J Natl Cancer Inst 2014;106:1–4.
32. Valentijn LJ, Koster J, Zwijnenburg DA, Hasselt NE, van Sluis P, Volckmann R, et al. TERT rearrangements are frequent in neuroblastoma and identify aggressive tumors. Nat Genet 2015;47:1411–4.